ACS APPLIED MATERIALS & INTERFACES

Research Article

www.acsami.org

Biocompatible Magnetite/Gold Nanohybrid Contrast Agents via Green Chemistry for MRI and CT Bioimaging

Sreeja Narayanan, Binulal N. Sathy, Ullas Mony, Manzoor Koyakutty, Shantikumar V. Nair, and Deepthy Menon*

Amrita Centre for Nanosciences and Molecular Medicine, Amrita Vishwavidyapeetham University, Kochi- 682041, Kerala

Supporting Information

ABSTRACT: Magnetite/gold (Fe_3O_4/Au) hybrid nanoparticles were synthesized from a single iron precursor (ferric chloride) through a green chemistry route using grape seed proanthocyanidin as the reducing agent. Structural and physicochemical characterization proved the nanohybrid to be crystalline, with spherical morphology and size ~35 nm. Magnetic resonance imaging and magnetization studies revealed that the Fe_3O_4 component of the hybrid provided superparamagnetism, with dark T_2 contrast and high relaxivity (124.2 ± 3.02 mM^{-1} s^{-1}). Phantom computed tomographic imaging demonstrated good X-ray contrast, which can be attributed to the presence of the nanogold component in the hybrid. Considering the potential application of this bimodal nanoconstruct for stem cell tracking and imaging, we have conducted compatibility studies on human Mesenchymal Stem Cells (hMSCs), wherein cell viability, apoptosis, and intracellular reactive oxygen species (ROS) generation due to the particle−cell interaction were asessed. It was noted that the material showed good biocompatibility even for high concentrations of 500 μg/mL and up to 48 h incubation, with no apoptotic signals or ROS generation. Cellular uptake of the nanomaterial was visualized using confocal microscopy and prussian blue staining. The presence of the nanohybrids were clearly visualized in the intracytoplasmic region of the cell, which is desirable for efficient imaging of stem cells in addition to the cytocompatible nature of the hybrids. Our work is a good demonstrative example of the use of green aqueous chemistry through the employment of phytochemicals for the room temperature synthesis of complex hybrid nanomaterials with multimodal functionalities.

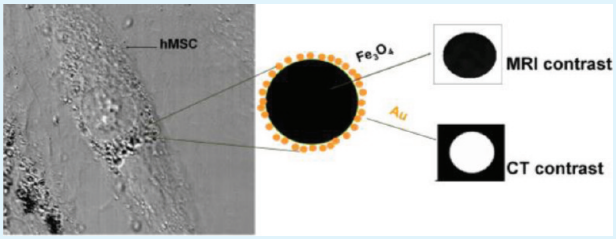

KEYWORDS: *iron oxide, gold, green synthesis, hybrid nanoparticles, MRI, CT, stem cells, imaging*

INTRODUCTION

Hybrid nanostructures have stirred great interest in the field of nanomedicine because of their diverse physicochemical properties and the consequent broad spectrum of biomedical applications including ultrasensitive detection, medical imaging, targeted therapeutics, etc.[1] Combinations of multiple components on a nanometer scale enabling integrated functionalities, has become one of the major advances in nanobiotechnology, such as in molecular diagnosis. In such a hybrid structure, iron oxide nanoparticles are important components enabling its use as T_2-weighted contrast agents in magnetic resonance imaging (MRI) and MR angiography, because of its superparamagnetic behavior.[2] These magnetic nanoparticles have been used in combination with fluorescent dyes, quantum dots, or plasmonic nanocrystals, aiding multimodal imaging functionalities.[3−6] Gold seems to be a better candidate in such composite nanostructures because of its nonreactivity and biocompatibility, unlike quantum dots or fluorescent dyes which have inherent limitations for in vivo use.[7,8] Colloidal gold (Au) has also recently gained impetus as blood-pool X-ray contrast agents for computed tomography (CT), in lieu of the conventional iodine based CT contrast agents.[9] Combining such distinct materials as iron oxide (Fe_3O_4) and gold (Au) at the nanoscale within a single entity can provide a nanohybrid having integrated MRI and CT functionalities for molecular diagnosis.

Current trends in nanomaterial synthesis allow preparation of such hybrid nanoconstructs with a variety of architectures such as core−shell, dumbbell, nanorice, nanoflower, etc. through organic routes at high temperature and energy consuming procedures.[10−13] This would hamper their biological use without postsynthesis processing and render the procedure not amenable to economic industrial scale-ups. Hence, an aqueous green chemistry approach for preparing biocompatible hybrid nanostructures with controllable sizes, monodispersities and dispersibility in physiological media is very demanding. Very recently, Kim et. al have reported the preparation of iron oxide/gold hybrid nanoparticles as MRI/CT dual contrast agent through thermal decomposition route followed by emulsification for providing an amphiphilic polymer coating.[14] However, green routes for preparing such hybrid nanoparticles have been less explored.

Emerging trends in the use of antioxidant plant-derived polyphenols as strong reducing agents in the synthesis of

Received: September 26, 2011
Accepted: November 22, 2011
Published: November 22, 2011

plasmonic nanoparticles of gold, silver, palladium, and copper propose them as potential alternatives to chemical reducing agents.[15−20] The hydrogen-donating property of hydroxyl groups[21] in the polyphenolic structure of such molecules helps to facilitate synergistic reduction and stabilization of the nanoparticles, thereby shielding them from agglomeration. Although remarkable progress has been made in preparing individual metallic nanoparticles using polyphenols, it has not yet been explored for the synthesis of any hybrid nanostructures. Hence, contrary to the routine chemical processess for preparing Fe_3O_4/Au hybrid nanoparticles, in this work, we report a green method of using one of the well-known polyphenols from grapes, viz., grape seed proanthocyanidin (GSP), to simultaneously aid reduction and stabilization of the nanohybrids at room temperature through a completely aqueous synthesis route. Abiding to the principles of green chemistry, glutathione, a tripeptide, was used to functionalize Fe_3O_4 nanoparticles before hybridizing with Au, to obtain a multicomponent nanosystem possessing superparamagnetism and CT contrast. These unique characteristics make this hybrid contrast agent ideally suited for simultaneous T_2-weighted MR imaging and X-ray imaging. Apart from these functional characteristics of the developed nanomaterial, the nanohybrids were tested on hMSCs as a model system for cytocompatibility and particle internalization studies, with a view of extending its potential for stem cell labeling and tracking.[22−24]

MATERIALS AND METHODS

Materials. Ferric chloride anhydrous was purchased from Merck. Grape Seed Proanthocyanidin (GSP) was obtained from BulkActives. Ammonia, Chloroauric acid and Glutathione were purchased from Qualigens, Spectrochem and Hi-media respectively. Sodium hydroxide was obtained from Hi-media. Milli-Q water was used throughout the experiments. All the chemicals were used as purchased.

Synthesis of Fe_3O_4 Nanoparticles, Glutathione Functionalization, and Its Quantification. Magnetite nanoparticles were synthesized at room temperature from a single precursor without any stabilizer through a completely aqueous route using the phytochemical grape seed proanthocyanidin. Briefly, 1 mL of 0.15 M ferric chloride was added to 2 mL of 10 mg/mL GSP and stirred for 5 min. The solution turned greenish-brown upon stirring. To this solution, 5−10 mL of 0.5% ammonia (or 0.5 M NaOH) was added and stirred for another 15 min. The resultant black precipitate was separated magnetically and washed thrice with double distilled water. The so formed magnetic nanoparticles suspended in water was further mixed with 3 mM L-glutathione under magnetic stirring. Additionally, higher concentrations of glutathione (6, 9, and 12 mM) were also used for capping magnetite nanoparticles (see the Supporting Information). The glutathione functionalized magnetic nanoparticles were separated through centrifugation. The supernatant from the above step was used to quantify the glutathione concentration using ninhydrin colorimetric method. Briefly, 2 mL of the supernatant was vortexed with 1 mL of 1% ninhydrin solution and heated in a water bath at boiling temperature, for 5 min. Upon reaction with the free amines in glutathione, ninhydrin resulted in a deep blue or purple color known as Ruhemann's purple,[25] which was spectrophotometrically analyzed at 570 nm. The concentration of glutathione in the supernatant was then deduced from the standard curve prepared for glutathione. The percentage of glutathione functionalized to the Fe_3O_4 nanoparticle surface was deciphered using the following mathematical expression:

$$\text{functionalized glutathione (\%)} = [(A_t - A_s)/A_t] \times 100 \quad (1)$$

where A_t is the total amount of glutathione used for functionalization; A_s is the amount of glutathione in the supernatant.

Synthesis of Fe_3O_4/Au Hybrid Nanoparticles. To facilitate the formation of magnetite-gold hybrid nanostructures, we resuspended glutathione functionalized Fe_3O_4 nanoparticles (2 mg/mL) into water and mixed with chloroauric acid (2.5 mM) under sonication for 5 min. Following this, a solution of GSP as the reducing agent for gold precursor, at a concentration of 200 μg/mL, was added and stirred for 2 h. The resultant hybrid nanoparticles were separated magnetically and washed thrice with double distilled water. The colloidal stability of the nanohybrids were evaluated in three different media, viz., water (pH 7), PBS (pH 7.2), and 0.5% BSA (pH 7) (see the Supporting Information).

Characterization of Fe_3O_4 /Au Hybrid Nanoparticles. The morphology and size of Fe_3O_4 and Fe_3O_4 /Au nanoparticles were examined using a FEI Tecnai T12 Transmission Electron Microscope (TEM, LaB6 gun, 120 kV). The aqueous dispersion of the particles at 1:10 dilution was drop-casted onto a carbon-coated copper grid and air-dried at room temperature before viewing under the microscope. The morphology of the hybrid nanoparticles was also visualized using Atomic Force Microscope (AFM, JSPM 5200, JEOL, Japan). The hydrodynamic particle size and size distribution was measured by the laser light scattering technique using a particle size analyzer (Nicomp Particle Size Analyzer 38/ZLS). The UV−vis spectra of Fe_3O_4 and Fe_3O_4/Au nanoparticles were measured using the Shimadzu UV−vis spectrophotometer (UV-1700 Pharma Spec). The phase structure and phase purity of the as-synthesized products were examined by a PANalytical XPert-pro X-ray diffractometer using Cu Ka radiation (λ = 1.5 Å), at an accelerating voltage and applied current of 36 kV and 20 mA respectively. Fourier Transform Infra-Red (FTIR) spectroscopy was used to identify the infrared absorption peaks, with the spectral scan set for the frequency range spanning from 4000 to 400 cm^{-1} using a Perkin-Elmer Spectrum RX-1 model. Material composition was analyzed by energy-dispersive X-ray spectroscopy (EDX, JEOL JSM-6490 LA). Elemental concentration of Fe and Au in the nanoparticles was quantified by Inductively coupled plasma atomic emission spectroscope (ICP-AES, Thermo Electron IRIS INTREPID II XSP DUO). The samples were microwave digested in ultra pure concentrated aqua regia before analysis. Magnetic measurements were carried out at room temperature on a Lakeshore-7410 vibrating sample magnetometry (VSM).

Magnetic Resonance (MR) and X-ray Contrast Imaging. Phantom agar MRI experiments were performed with a 1.5 T clinical Signa HDxt scanner (GE Health Care). T_2-weighted images were acquired using the following parameters: 1.5-T, fast spin echo, Repetition time TR = 2500, Echo time TE = 30−203 ms, FOV 16 cm^2, resolution 256 × 256 points and slice thickness = 6 mm. Suspensions of Fe_3O_4 and Fe_3O_4 /Au nanoparticles at varying concentrations of iron were prepared in PBS and set in 2% w/v agar solution at 80 °C in 0.5 mL microcentrifuge tubes. The phantom MR imaging studies were carried out with agar gel as the control.

X-ray contrast enhancement imaging of the hybrid nanoparticles was carried out using a clinical SOMATOM Sensation Cardiac 64 CT scanner (Siemens). To determine the contrast enhancement by virtue of the presence of gold in the hybrid, a tube voltage of 100 kVp and tube current of 200 μA were used, with a scan time of 6.97 s, slice thickness 5 mm, and rotation time 1 s. The data was analyzed by recording the Hounsfield units (HUs) for manually selected regions of interest.

Cell Culture Experiments. All cell culture reagents were purchased from Sigma Aldrich, USA, except otherwise mentioned. hMSCs were isolated from the bone marrow aspirates of normal healthy adult donors after informed patient consent and approval from the institutional ethical committee. The isolated cells were cultured in alpha minimal essential medium containing 20% fetal bovine serum (Stemcell Technologies, USA), penicillin−streptomycin 100 units/mL (Invitrogen, USA), and 2 mM L-glutamine as previously reported by us.[26] Cells from passages 2−3 were used for all the experiments.

Cytocompatibility Experiments. *i. Alamar Blue Assay.* Cytocompatibility of the nanoparticles in terms of cell viability was assessed by the Alamar blue assay.[27,28] hMSCs were seeded in 96-well plates with a seeding density of 2 × 10^3/well. Following cell

attachment, fresh medium containing different concentrations of Fe_3O_4 and Fe_3O_4 /Au nanoparticles was added and cells were incubated for 24 and 48 h. Cells cultured in 10% FBS containing media and in 1% Triton X100 were used as negative and the positive control respectively. After incubation, wells were washed twice with PBS and 10 μL of alamarBlue (Invitrogen, USA) and 100 μL of serum free medium was added to each well and incubated at 37 °C for 4 h. The optical density was recorded using a Power Wave XS microplate spectrophotometer (Biotek) at 570 nm, with 600 nm set as the reference. The cell viability percentage was calculated using the following equation

$$\text{cell viability}\ (\%) = (\text{Int}_s/\text{Int}_{\text{control}}) \times 100 \quad (2)$$

where Int_s is the OD value of the cells incubated with the NP suspension and $\text{Int}_{\text{control}}$ is the OD value of the cells incubated with the culture medium alone.

This was followed by the morphological analysis of the cells exposed to the hybrid nanoparticles. For this, the hMSCs were seeded in 6-well plates at a seeding density of 5×10^4 cells/well and allowed to attach following which the hybrid nanoparticles were added at a concentration of 500 μg/mL and incubated for 24 h at 37 °C. The labeled cells were then washed and trypsinized and were reseeded into separate 6-well plates allowing to be in culture for 24 h. Live digital images of the cells were obtained using an inverted microscope (Leica Microsystems).

ii. Annexin V Apoptosis Assay by Flow Cytometry. Annexin V-FITC apoptosis detection kit (Becton-Dickinson, USA) was used to validate the cytocompatibility of the nanoparticles by measuring the levels of apoptotic signals. Briefly, hMSCs treated with bare Fe_3O_4 and hybrid nanoparticles (250 μg/mL separately) for 24 h were trypsinized and centrifuged at 1500 g for 5 min. The cells were washed with phosphate buffered saline and resuspended in 250 μL of 1X binding buffer at a concentration of 2×10^5 cells/mL. To this suspension was added 5 μL of FITC-Annexin V and propidium iodide, and the solution was incubated in the dark for 15 min. 400 μL of 1× binding buffer was added to this suspension and analyzed immediately using a flow cytometer (FACS Aria II, Becton-Dickinson). Data from 10 000 events per sample were acquired.

iii. Intracellular Reactive Oxygen Species (ROS) Assay. Intracellular accumulation of ROS was determined with dichlorofluorescein-diacetate (H_2DCF-DA, Invitrogen, USA). This nonfluorescent compound accumulates within cells upon deacetylation. H_2DCF then reacts with ROS to form fluorescent 2,7-dichloroflurescein. hMSCs were trypsinized and seeded at a density of 2×10^5 cells/well into 6-well tissue-culture plates. After 10 h, medium was discarded and replaced with fresh medium containing bare and hybrid nanoparticles separately at similar concentration (250 μg/mL) as that used for apoptosis assay. After 24 h of incubation, cells were washed with PBS and incubated with 5 mM H_2DCF-DA (in 100% ethanol) at 37 °C for 30 min. The cells were then harvested and FACS analysis was performed. The intensity of fluorescence was detected with an excitation filter of 488 nm and band-pass emission filter of 530 ± 15 nm.

Cell Labeling. Cellular uptake of the hybrid nanoparticles by hMSCs was visualized by confocal microscopy, and for further validation Prussian blue histochemical staining was performed.

i. Confocal Microscopy. hMSCs were seeded on 13 mm glass coverslips placed inside a 24-well tissue culture plate at a seeding density of 1000 cells/coverslip. After 24 h, the adherent cells were washed with PBS and replaced with media containing Fe_3O_4 /Au nanoparticles and thereafter incubated for 24 h at 37 °C. The cells were further washed with PBS to completely remove loosely attached and free particles in the medium. Fixation of the cells was done using 2% paraformaldehyde. The coverslips were then mounted with DPX mounting medium and DIC images were obtained using a Leica SP5II inverted confocal microscope (Leica Microsystems).

ii. Prussian Blue Staining. hMSCs treated with the hybrid nanoparticles were fixed with 2% formaldehyde and washed with PBS, followed by incubation with 2% potassium ferrocyanide (Sigma, USA) in 6% hydrochloric acid for 25 min. After washing, the samples were then examined under a light microscope (Leica Microsystems).

RESULTS AND DISCUSSION

Mechanism of Green Synthesis. In the present study, magnetite nanoparticles were prior synthesized and further functionalized with glutathione, followed by conjugation with

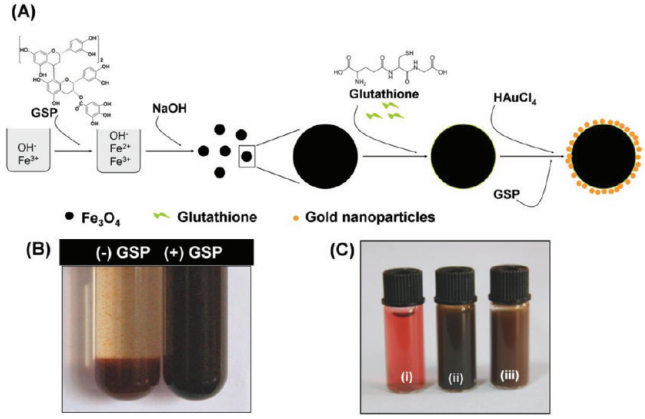

Figure 1. (A) Schematic illustration depicting the stepwise preparation of Fe_3O_4/Au hybrid nanoparticles through green route. (B) Photographic images of the precipitate obtained in the absence (-GSP) and presence (+GSP) of GSP during Fe_3O_4 nanoparticle preparation and (C) Photographic images of GSP-derived (i) Au nanoparticles, (ii) Fe_3O_4 nanoparticles, (iii) Fe_3O_4/Au hybrid nanoparticles.

gold, without the use of any extra stabilizing agent as depicted in Figure 1A. This synthesis route used ferric chloride as the only iron precursor, which was partially reduced using GSP, a mild, nontoxic reducing agent to yield ferrous ions at room temperature. This partial reduction was indicated by a color change from yellow to a greenish-brown tinge. Without the aid of any chemical reducing agents, but the polyphenol GSP, Fe^{2+} and Fe^{3+} were coprecipitated at an alkaline pH (aided by the addition of 0.5 M NaOH or 0.5% NH_3) yielding a black suspension of magnetite as shown in Figure 1B. GSP used in this experiment provided both reducing and stabilizing effects to the formed nanoparticles. Experiments carried out without the addition of GSP, resulted in only a dull brown nonmagnetic precipitate, thereby confirming the reducing potential of GSP in this protocol, as shown in Figure 1B. Thus, our results illustrate that GSP provides strong reduction of the precursors even at room temperature.

To functionalize the surface of the magnetite nanoparticles for preparing a nanohybrid with gold, we selected glutathione as the linker molecule. Gluthathione is a tripeptide which has a cysteine residue flanged by glutamic acid. The presence of multiple functional groups (carboxyl, amine and thiol) in glutathione endows it with attractive possibilities of bioconjugation with various molecules of interest. Various researchers have used glutathione capping on gold nanoparticles as well as quantum dot-magnetite nanohybrid.[3,29,30] In our synthesis strategy, we have utilized the thiol moiety of glutathione to facilitate binding of gold to the surface of glutathione functionalized Fe_3O_4 nanoparticles. It is important to note that all these reactions were carried out at room temperature, which helped to maintain the chemical integrity of the peptide linker. Au hybridization with Fe_3O_4 was done by an in situ reduction of gold precursor ($HAuCl_4$) by GSP over glutathione

dx.doi.org/10.1021/am201311c | ACS Appl. Mater. Interfaces 2012, 4, 251–260

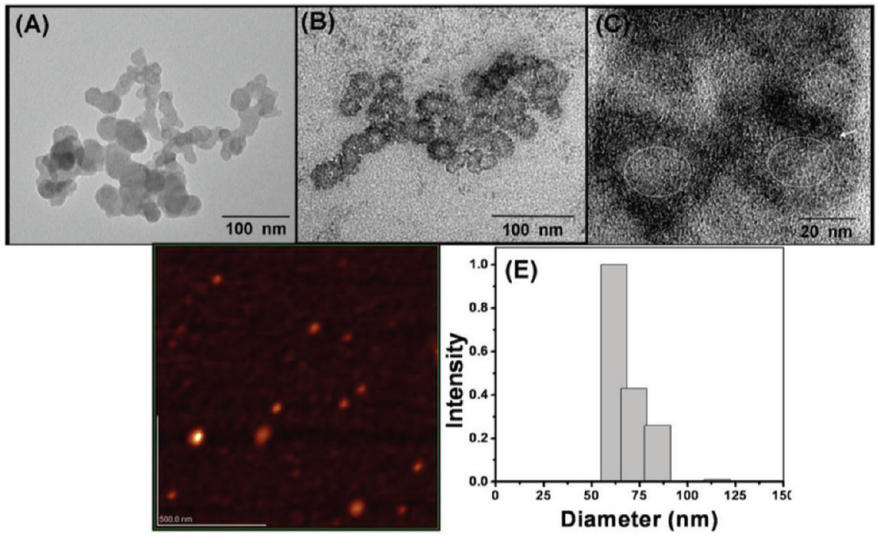

Figure 2. TEM images of (A) bare Fe_3O_4 nanoparticles, (B) Fe_3O_4/Au hybrid nanoparticles and (C) magnified image of hybrid nanoparticles clearly showing a coating of gold nanoparticles over magnetite. Arrow-head points toward gold and dotted circle depicts the inner magnetite core. (D) AFM image of hybrid showing particles with average size ~35 nm and (E) DLS data showing the hydrodynamic particle size distribution (>90%) around 55 ± 25 nm.

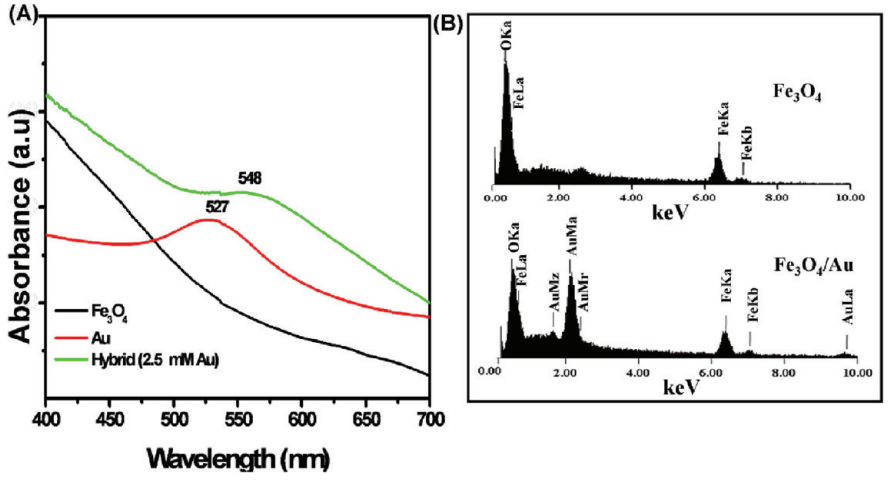

Figure 3. (A) UV−vis absorption spectra and (B) EDAX spectra of Fe_3O_4 and Fe_3O_4/Au hybrid nanoparticles.

functionalized Fe_3O_4 nanoparticles. Formation of the hybrid was indicated by a color change from black to brownish-black as seen in Figure 1C. Bare gold nanoparticles prepared using GSP as the reducing agent showed a pale red color (Figure 1Ci). Nanohybrids were then separated magnetically for physicochemical characterization.

Nanoparticle Characterization. The size, morphology, and particle size distribution of the synthesized nanoparticles were evaluated using TEM, AFM and dynamic light scattering (DLS) respectively. TEM observations of the samples shown in Figure 2 revealed that Fe_3O_4 nanoparticles were ~30 nm in size, while the hybrid size increased to ~35 nm upon conjugation with nanogold. Figure 2C clearly indicates the nanohybrid formation with nanogold over the magnetic core. Both TEM and AFM images showed that the overall morphology of the hybrid nanoparticles was spherical. The particle size of the nanohybrid measured by DLS was nearly 55 ± 25 nm, it being the hydrodynamic diameter in suspension (Figure 2E).

To further confirm the formation of the nanohybrid, surface plasmon resonance (SPR) of nanogold in the hybrid was spectrophotometrically recorded (Figure 3A). It was observed that Au nanoparticles prepared using GSP as the reducing agent showed an SPR band peaking at 527 nm, while Fe_3O_4 nanoparticles did not reveal any absorption bands in the visible region of the spectrum. However, hybrid Fe_3O_4/Au nanoparticles showed a visible red shift of the SPR band to 548 nm. Similar observations on varying optical absorption bands have been reported for iron oxide/gold hybrids prepared using nonaqueous chemical routes.[31−33] Coating of the dielectric iron oxide core with optically active gold leads to this shift of the SPR frequency, the position of which can be controlled by varying the thickness of the gold coating and core diameter.[10,34]

An elemental compositional analysis of bare and hybrid nanoparticles was performed using EDX spectroscopy and ICP-AES which further validated the formation of the hybrids. EDX spectra of bare and hybrid nanoparticles revealed the presence of iron and gold giving good support to the formation of the hybrid structure (Figure 3B). ICP-AES analysis was used to

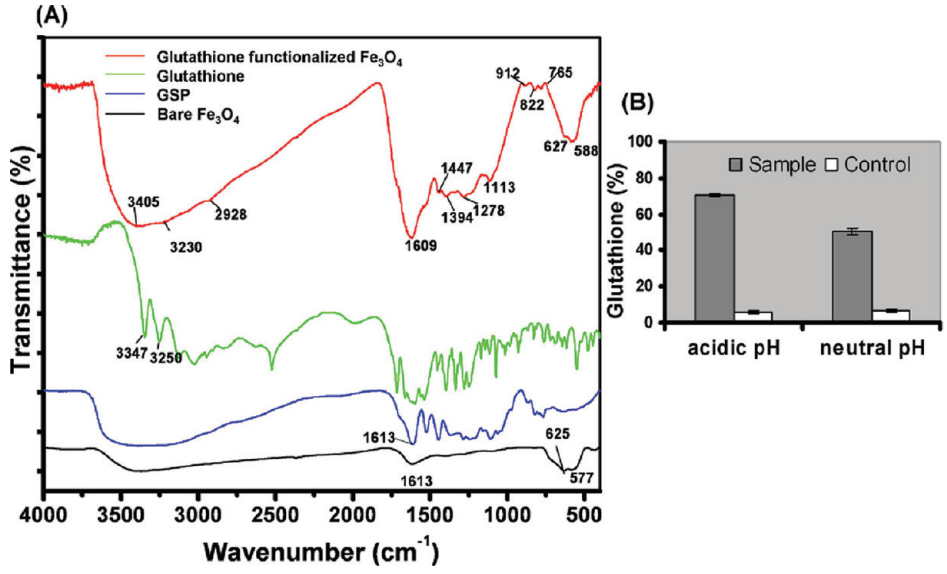

Figure 4. (A) FTIR spectra of Fe_3O_4 nanoparticles, GSP, glutathione and glutathione-functionalized Fe_3O_4 nanoparticles. (B) Ninhydrin protein assay results showing the effect of pH on glutathione functionalization of Fe_3O_4 nanoparticles.

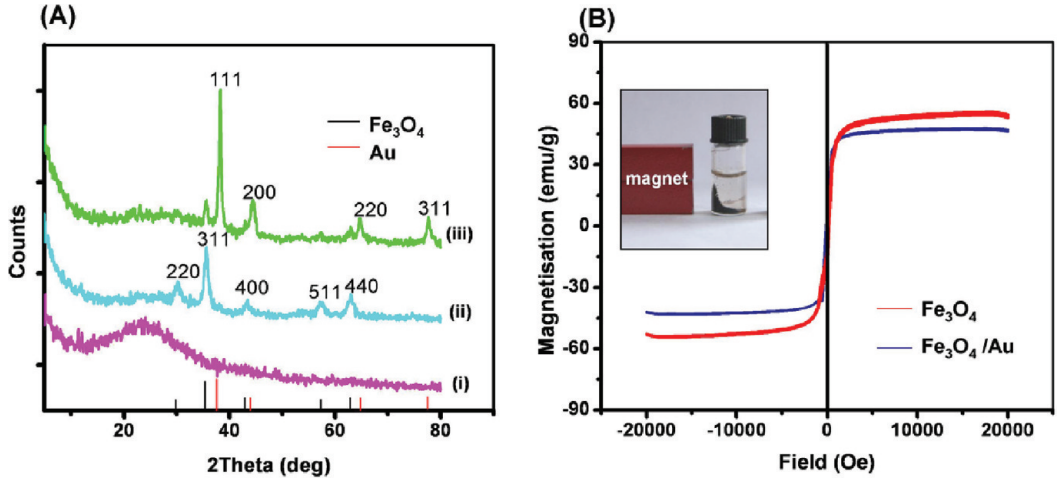

Figure 5. (A) Powder X-ray diffraction patterns: (i) experiment done without GSP, (ii) Fe_3O_4 nanoparticles prepared using GSP, and (iii) Fe_3O_4/Au hybrid nanoparticles prepared using GSP; and (B) magnetization curve of Fe_3O_4 and Fe_3O_4/Au hybrid nanoparticles. Inset in B shows hybrids separated by an externally placed bar magnet.

quantify the concentration of iron and gold in the nanohybrid. The concentration values mentioned hereafter for iron and gold have been estimated from the ICP-AES data.

FTIR spectroscopy (Figure 4A) was used to confirm the formation of iron oxide as well as its conjugation with glutathione. FTIR spectrum of bare Fe_3O_4 shown in the figure indicates the characteristic vibrations of Fe−O from a tetrahedral site at 625 cm^{-1} and from an octahedral site at 577 cm^{-1}.[35] The broad peak occurring between 3500 and 3200 cm^{-1} corresponds to hydrogen bonded O−H stretch and a comparatively narrower peak at 1613 cm^{-1} due to C−C=C symmetric stretch indicates the presence of polyphenolic GSP on Fe_3O_4 nanoparticles, which possibly provides a stabilizing effect to the nanoparticles. Glutathione functionalized Fe_3O_4 nanoparticles showed peaks at 3405 and 3230 cm^{-1} corresponding to N−H stretch and a peak at 1447 cm^{-1} due to N−H bend. The narrowing as well as increased intensity of the peak at 1609 cm^{-1} indicates the collective signals from the aromatic ring of surface polyphenols, N−H bends and C=O stretches of amide bonds in glutathione as well as the presence of hydrogen bond formation between the polyphenols on Fe_3O_4 nanoparticles and glutathione molecules. The peaks at 765 and 910 cm^{-1} can be attributed to the −SH of glutathione and the aromatic ring structure of polyphenols respectively in functionalized Fe_3O_4 nanoparticles. The presence of glutathione on Fe_3O_4 should also have resulted in a sharper peak at 2500−2400 cm^{-1} corresponding to the −SH stretching vibration. The absence of this may be attributed to the lower concentration of glutathione (3 mM) used to stabilize the nanoparticles in the current protocol. However, a sharp peak in this frequency range was clearly evident for increasing glutathione content (>9 mM), which yielded agglomerated nanoparticles (see the Supporting Information). The broadening of the peak in the 3500−3100 cm^{-1} range can be attributed to the intermolecular hydrogen bond formation between glutathione and polyphenols and the steric hindrance because of the bulky groups in GSP. The occurrence of the Fe−O peaks (627, 588 cm^{-1}, although with slight shift) in

dx.doi.org/10.1021/am201311c | ACS Appl. Mater. Interfaces 2012, 4, 251−260

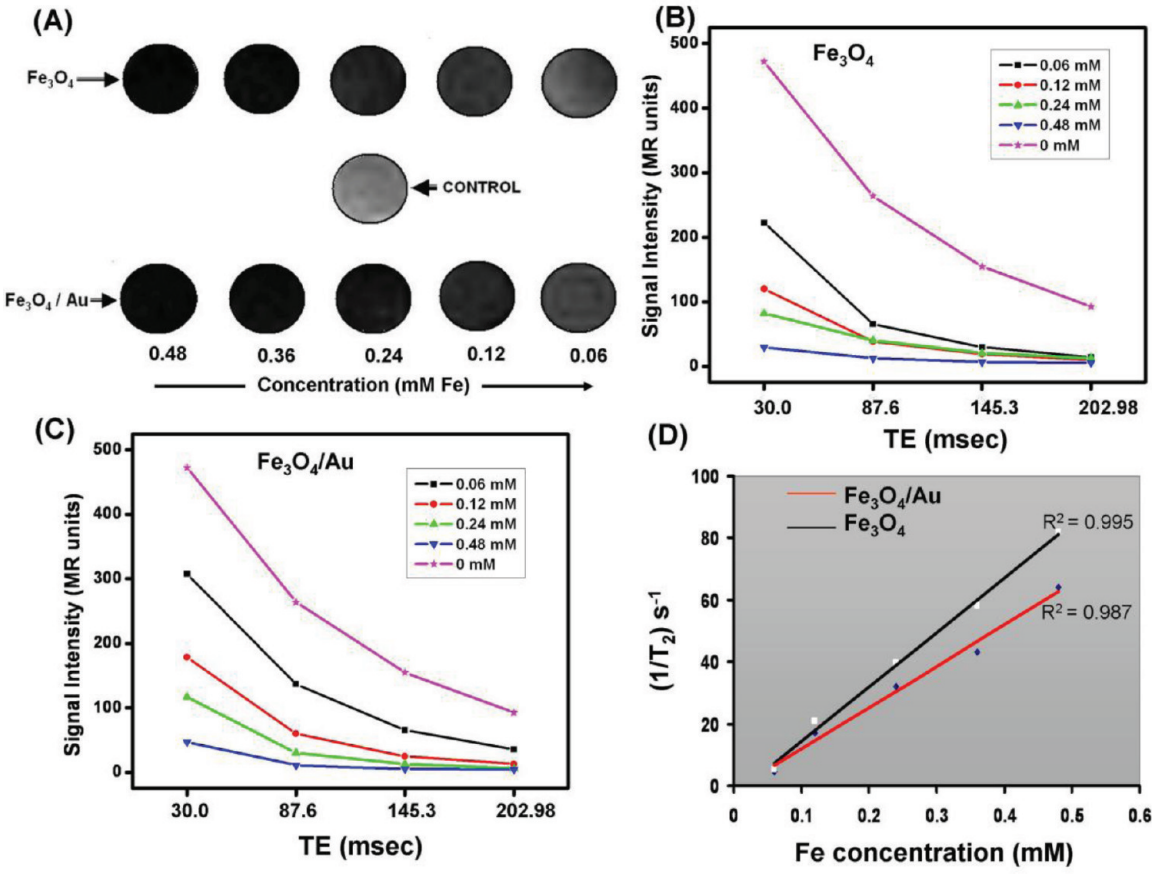

Figure 6. MRI imaging. (A) T_2-weighted MR phantom images of Fe_3O_4 and Fe_3O_4/Au hybrid nanoparticles with reference to control. (B, C) Signal intensity vs TE plots for Fe_3O_4 and Fe_3O_4/Au hybrid nanoparticles, respectively; and (D) T_2 relaxation rate ($1/T_2$) plotted against varying Fe concentrations.

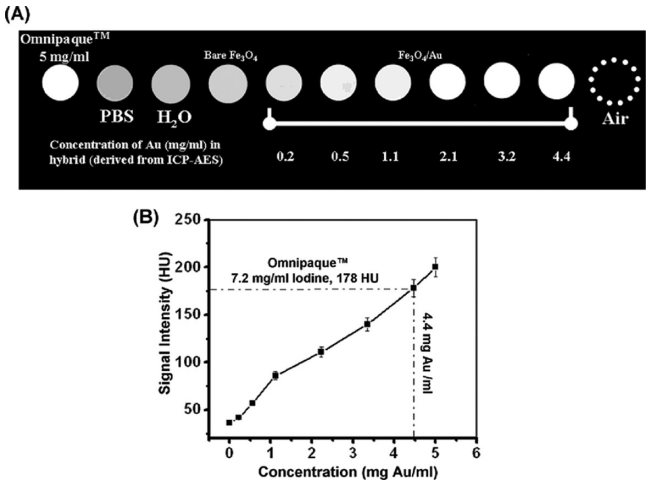

Figure 7. CT imaging of the hybrid nanoparticles. (A) CT images of the phantoms at 100 kVp with reference to control samples. (B) Au concentration (in hybrid nanoparticles) vs HU plot showing linear dependence.

glutathione functionalized Fe_3O_4 indicates that the conjugation has not altered the integrity of Fe_3O_4 nanoparticles that aids its magnetism.

The glutathione content associated with Fe_3O_4 nanoparticles was quantified using the ninhydrin protein assay. Concentration of glutathione (in percentage of the total amount used for the experiment) on Fe_3O_4 nanoparticles after the functionalization carried out in acidic or neutral pH conditions was calculated to be 70.6 and 50.2%, respectively (Figure 4B). The comparatively higher glutathione content in acidic pH may be indicative of a higher possibility of electrostatic interaction between the stabilizer polyphenols and glutathione at reduced pH, aiding better association.

The XRD analysis was carried out to determine the phase crystallinity and purity of the synthesized nanoparticles. Figure 5A gives the XRD patterns of bare as well as Fe_3O_4/Au nanoparticles. For samples prepared without the addition of GSP, no crystalline peaks of Fe_3O_4 nanoparticles were obtained as can be seen from the XRD pattern in (i). This clearly points to the role of GSP in the formation of crystalline Fe_3O_4 nanoparticles. The pattern in (ii) gives the XRD of crystalline inverse spinel structured Fe_3O_4 nanoparticles prepared using GSP. The diffraction peaks at 2θ = 30.1° (220), 35.5° (311), 43.2° (400), 57.0° (511), and 62.8° (440) indicated magnetite formation. The spectrum shown in (iii) represent the formation of the nanohybrid and clearly shows the evolution of Au peaks. As evident from the pattern, the diffraction peaks arising from the fcc structure of Au with peak positions at 2θ = 38.3° (111), 44.56° (200), 65.01° (220) and 78.42° (311) dominates over the Fe_3O_4 reflections in the hybrid nanoparticles. This can be attributed to the heavy atom effect of Au that hinders the diffraction peaks of Fe_3O_4.[31] XRD spectra thus provide a clear support for the formation of Fe_3O_4 and the hybrid nanoparticles.

dx.doi.org/10.1021/am201311c | ACS Appl. Mater. Interfaces 2012, 4, 251–260

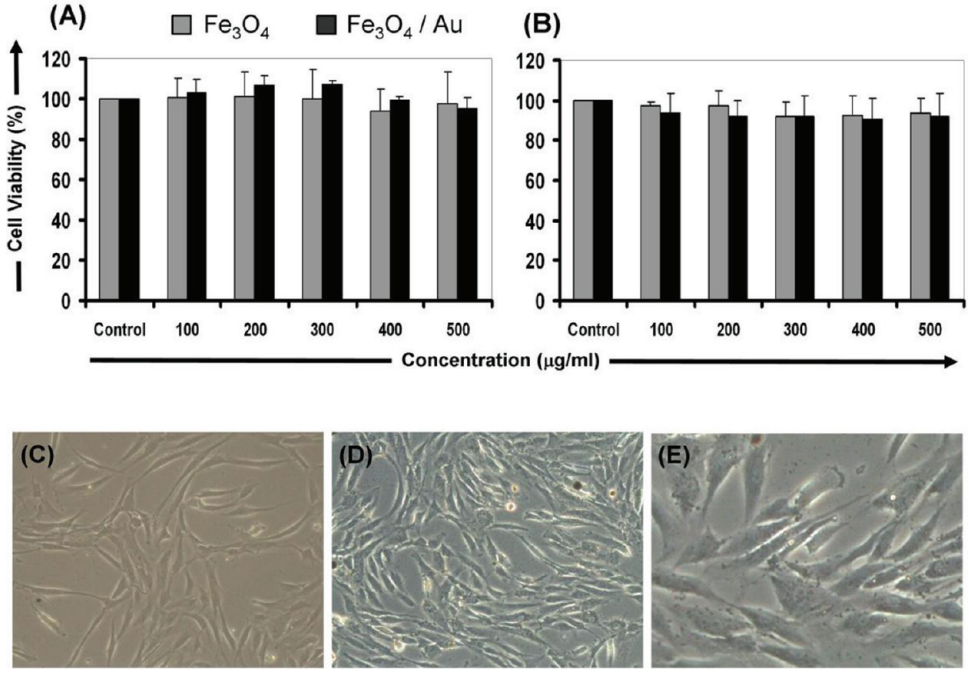

Figure 8. Cell viability using Alamar blue. hMSCs treated for (A) 24 and (B) 48 h with Fe_3O_4 and Fe_3O_4/Au hybrid nanoparticles separately. The values represent the mean ± standard deviation of three independent experiments. Optical microscopy images of hMSCs in culture (C) unexposed to nanoparticles (control), (D) cells reseeded after hybrid nanoparticle exposure, and (E) magnified image of cells in D.

Magnetization Measurements. Superparamagnetic iron oxide nanoparticles (SPIONs) are important in magnetic imaging owing to their magnetic susceptibility far exceeding that of conventional T_1 contrast paramagnetic materials such as Gadolinium chelates.[24] Accordingly, we evaluated the magnetization property of bare and hybrid Fe_3O_4/Au nanoparticles by measuring its magnetization saturation using VSM at room temperature. Illustrated in Figure 5B is the magnetization curve for bare Fe_3O_4 and Fe_3O_4/Au nanoparticles. The anhysterical, sigmoidal curve with lack of coercivity and remanence in magnetization, confirms the superparamagnetic nature of the as-synthesized bare and hybrid samples. The saturation magnetization (M_s) value of Fe_3O_4 nanoparticles was measured to be 56.57 emu/g at 25 °C. However, the magnetization reduced to 48.6 emu/g for the nanohybrids chiefly owing to the diamagnetic behavior of Au. The inset in Figure 5B clearly shows that the synthesized hybrid nanoparticles were capable of magnetic separation using an external bar magnet. Our magnetic measurement results suggest that use of innovative green routes of synthesis could yield equally proficient SPIONs as those obtained from conventional chemical processes.

Phantom MR and X-ray Imaging Studies. Subsequently, the MR contrast capability of bare and hybrid nanoparticles was tested using a 1.5T clinical MRI system by the spin−echo method. Phantom agar gels were prepared with varying concentrations of Fe_3O_4 nanoparticles equivalent to 0.06, 0.12, 0.24, 0.36, 0.48 mM of Fe (quantitatively estimated using ICP-AES), with agar gel as the control. On evaluating the T_2-weighted images of bare and hybrid Fe_3O_4/Au nanoparticles in the phantom gels, a noticeable darkening (with decreasing signal intensity) and thereby negative contrast was observed with increasing Fe concentrations (Figure 6A−C). Although the trend in the concentration v/s signal intensity curves were similar for both hybrid and bare nanoparticles, a better dark contrast was shown by the latter when compared with control agar gel. It was further observed that the relaxation rate ($1/T_2$) varied linearly with iron content (as shown in Figure 6D) according to the following formula

$$\frac{1}{T_2} = \frac{1}{T_2^0} + R_2 C \tag{3}$$

where $1/T_2$ is the measured transverse relaxation rate in the presence of nanoparticles, $1/T_2^0$ is the relaxation rate of control agar gel and C represents the Fe concentration in nanoparticles. The transverse relaxivity R_2 (which corresponds to the slope of the lines in Figure 6D) measured at 1.5T was estimated to be 161 ± 2.48 $mM^{-1}s^{-1}$ and 124.2 ± 3.02 $mM^{-1}s^{-1}$ respectively for the bare and hybrid SPIONs. The relaxivity values for our green nanoparticles are significantly higher in comparison to the R_2 of commercially available Resovist SPIO nanoparticles which is reported to be 82 ± 6.2 mM^{-1} s^{-1} at 1.5T.[36] The MR relaxivity data obtained in this experiment was also in agreement with the magnetization data recorded using VSM, indicating that both bare and hybrid nanoparticles showed excellent superparamagnetic characteristics.

To study the feasibility of the hybrid nanoparticles as X-ray contrast agents, we imaged the samples using a clinical CT scanner at a tube voltage of 100 kV_p for a scan time of 6.97 s. We compared the X-ray absorption of the hybrids with Omnipaque, a popular iodine-based CT contrast agent currently used in the clinic. Figure 7A depicts the phantom images obtained for varying concentrations of the hybrid prepared in PBS, with bare Fe_3O_4, Omnipaque, PBS, water and air set as controls. Hounsfield Unit (HU) values were obtained from selected regions of interest (ROIs) for each sample for increasing content of gold in the hybrid. Figure 7B shows that 4.4 mg Au/ml contained in the Fe_3O_4/Au hybrid gave an equivalent X-ray absorption as 7.2 mg/mL Iodine in Omnipaque (viz., 178 HU). This corresponds to an X-ray attentuation nearly 1.6 times that of the iodine contrast agent,

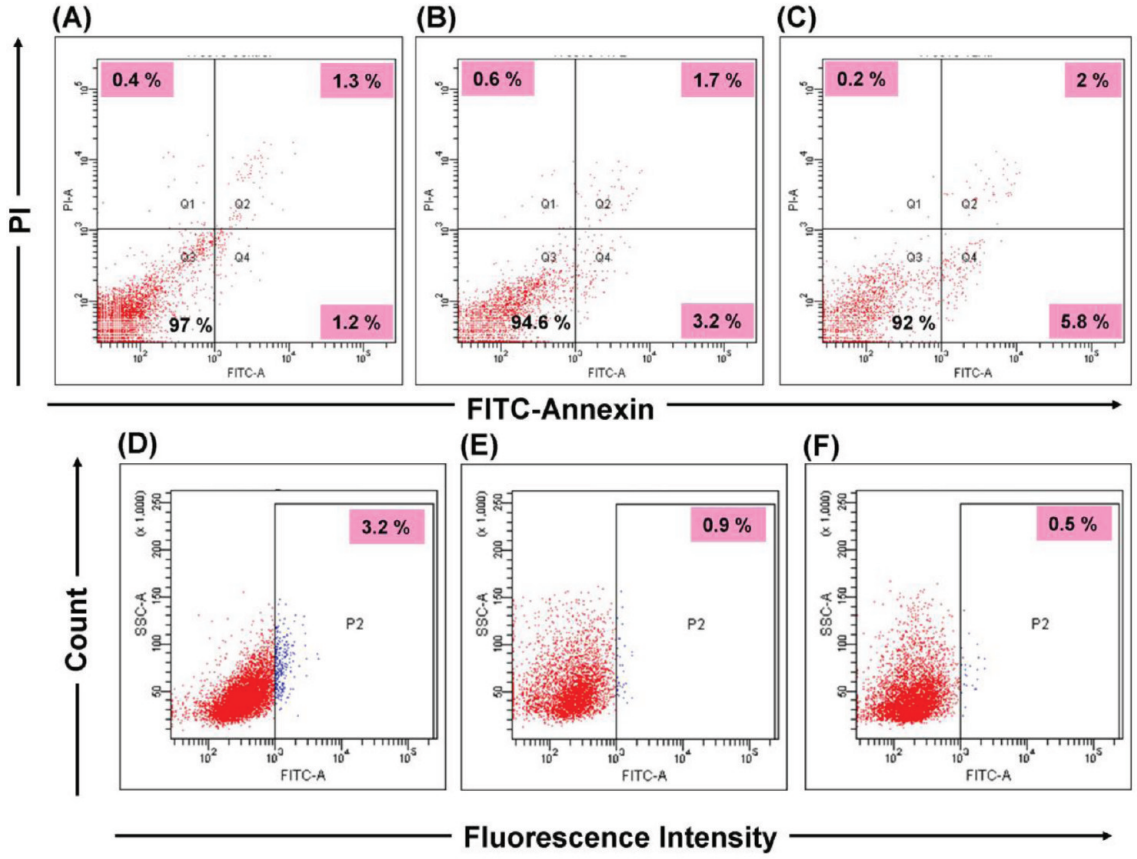

Figure 9. Representative FACS plots showing results of apoptosis and ROS assay. Upper panel shows Annexin−V-PI staining assay where (A) Unlabeled cells, (B) Fe_3O_4 and (C) Fe_3O_4/Au hybrid nanoparticle treated cells. The different labeling patterns in this assay identify the different cell fractions, i.e., PI-negative/Annexin V-negative viable cells (Q3), PI-negative/Annexin V-positive apoptotic cells (Q4), PI-positive/Annexin V-positive late apoptotic cells (Q2), and PI-positive/Annexin V-negative necrotic cells (Q1). Lower panel shows intracellular ROS flowcytometric measurements done on hMSCs treated with the nanoparticles using dichlorofluorescein-diacetate assay where (D) Unlabeled negative control cells. The minor ROS percentage is the inherent intracellular ROS in hMSCs, (E) Fe_3O_4, and (F) hybrid nanoparticle treated cells showing insignificant levels of ROS.

which could be attributed to the presence of electron dense nanogold in the hybrid. Gold has a higher atomic number and electron density (79 and 19.32 g/cm^3, respectively) in comparison to that of iodine (53 and 4.9 g/cm^3) contributing to this effect.[37] Thus, in lieu of the conventional iodinated materials, zirconium dioxide or barium sulfate contrast agents used in CT whose toxicity issues are a big concern,[38] we propose the use of a biocompatible nanomaterial prepared through green routes, with high X-ray attenuation complemented with their magnetic contrast. Experiments were also performed to evaluate the CT contrast of gold nanoparticles prepared using GSP as the reducing agent (Au nanoparticles as shown in Figure 1Ci). However, bare nanoAu gave a CT signal intensity of 354 HU for a concentration of 5 mg/mL, which was nearly 2-fold higher in comparison to the hybrid sample at its highest concentration.

Cytotoxicity Experiments. The practical clinical applications of many of the nano contrast agents are limited by their toxicity. Clinically approved SPIONs are normally surface stabilized with dextran, starch, albumin or other polymeric coatings to prevent nanoparticle aggregation and improve surface biocompatibility.[39] However, their large overall size because of coating may significantly limit tissue distribution, intracellular penetration, intravenous delivery, and metabolic clearance. Apart from coatings, polycationic transfecting agents such as poly-L-lysine are complexed with SPIONs to increase their chances of cell penetration for the ease of labeling stem cells. These chemical agents have narrow tolerated concentrations and are not approved by the FDA for clinical use.[40] Accordingly, our intention was to evaluate the cytocompatibility of the GSP stabilized nanoparticles on human mesenchymal stem cells, with a view to extend its applicability for stem cell labeling and tracking using the dual modalities of MRI and CT.

Alamar blue based cytotoxicity assay was performed on hMSCs by incubating with both bare magnetite and hybrid nanoparticles separately in the concentration range of 100−500 μg/mL. It is evident from paenls A and B in Figure 8 that bare as well as hybrid nanoparticles showed no significant reduction in cell viability of hMSCs, even at relatively high dosages and prolonged incubation time of 48 h. A morphological analysis of hMSCs treated with the hybrid nanoconstructs at a high dosage of 500 μg/mL for 24 h was done by optical microscopy (Figure 8C−E). The images revealed that even after exposure to a high concentration of the nanohybrids, the reseeded cells were viable, well spread and appeared to be morphologically intact. This agrees well with the results obtained from the cytotoxicity experiments and can be considered as a good supporting evidence to the biocompatible nature of the diagnostic nanoprobe. It indicated that the green-synthesized nano-

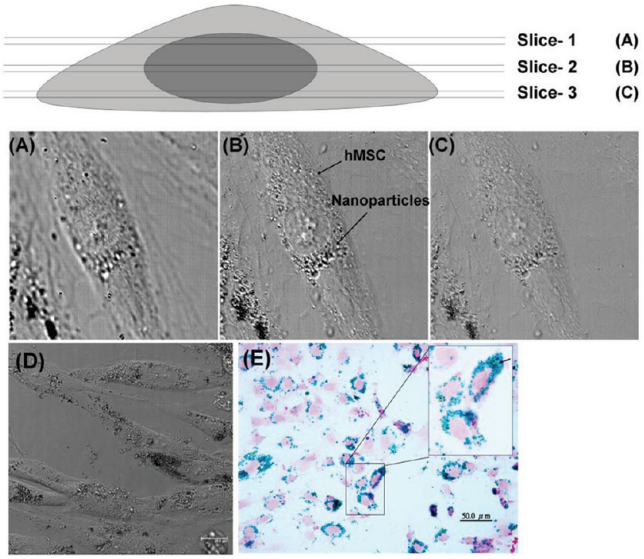

Figure 10. DIC images of hMSCs taken using confocal microscope. (A–C) Serial optical sections of hMSCs showing hybrid nanoparticles distributed in the cytosol upon uptake. (D) Low magnified DIC image of hMSCs showing nanoparticle uptake, and (E) Prussian blue staining performed on hMSCs showing the uptake of hybrid nanoparticles as blue stain. Arrow-head indicates magnetite nanoparticles stained with prussian blue.

particles would be a safer option for in vivo experiments as the stem cell viability was not compromised even at concentrations as high as 500 μg/mL, which probably is much higher than that encountered in vivo.

In addition to the metabolic acitivity, it was relevant to assess if the nanoprobes induced any apoptotic changes to hMSCs after a prolonged exposue (24 h) at a relatively high concentration of 250 μg/mL. Flow cytometry based annexin V staining assay was performed for this purpose. hMSCs treated with both bare and hybrid SPIONs separately were stained with FITC-annexinV that reacts only with the externalized phosphatidylserine of cells which have undergone apoptosis.[41] The red fluorescent propidium iodide (PI) dye stains the nucleus of the late-stage apoptotic and dead cells owing to their permeable membranes. Interestingly, no obvious signs of apoptosis were observed in the treated cells as evident from the dot-plot obtained from the FACS analysis (Figure 9A–C). Incubation with the nanoparticles did not appear to significantly affect the cells and an appreciable percentage (>90%) of cells was found viable after incubation. This corroborated well with the Alamar blue assay where a similar viability trend was observed.

Considering the major objective of synthesizing cell-friendly multifunctional hybrid nanoparticles, intracellular ROS was also quantified using flowcytometry, with an ROS sensor H_2DCF-DA. The assay was performed at a concentration of 250 μg/mL, to reconfirm the biocompatibility of our nanomaterial on hMSCs. Figure 9D-9F show the results of ROS assay, depicting insignificant ROS levels in nanoparticle treated cells even at this high concentration, indicating that the nanomaterials do not contribute to any additional stress to the cells. Interestingly noticed was the slight decrease in ROS levels in the nanomaterial treated cells compared to the control. Considering earlier studies pertaining to the antioxidant and ROS scavenging properties of proanthocyanidin,[42−44] we propose that a probable reason for the decrease in ROS levels in the nanoparticle treated hMSCs could be the ROS scavenging effect of the stabilizer proanthocyanidin. Thus, we strongly anticipate that effectively controlling the availability of the antioxidant proanthocyanidin associated with the nanoparticles, these nanoconstructs could be attractive "theranostic" agents with both therapeutic and diagnostic capabilities.

Intracellular Uptake. Cellular uptake of the hybrid nanoparticles by hMSCs was investigated using confocal microscopy and histochemical staining and is shown in Figure 10. Serial optical sections of the cells incubated with nanoparticles revealed a clear intracytoplasmic distribution of the particles following cellular uptake as depicted in Figure 10A–D. Polyphenols are known to associate well with the plasma membrane microdomains[45] and thus we hypothesize that the stabilizer polyphenols in the nanohybrids would have played a vital role in the entry of the nanoparticles into the cells. Prussian blue histochemical staining performed to detect the iron content in the intracytoplasm of cells, helped to validate the presence of iron oxide nanoparticles within cells, indicated by a blue hue. Figure 10E depicts the uptake of hybrid nanoparticles abundantly into the cellular cytoplasm. This corroborates well with the confocal results on cellular uptake by hMSCs. These hybrid nanoconstructs when appropriately internalized by the hMSCs can assist their detection through both magnetic and CT modalities.

CONCLUDING REMARKS

In conclusion, we report a simple green synthesis route for preparing multimodal nanohybrids based on Fe_3O_4/Au possessing magnetic and X-ray contrast properties. Unlike various available reports on hybrid nanoparticles, this synthesis scheme is unique and advantageous in that it utilizes single precursors of iron and gold and a green chemical (grape seed proanthocyanin) for reduction as well as stabilization of the nanohybrids at room temperature. These nanohybrids displayed superparamagnetism with high magnetic saturation and relaxivity. The simple combination of gold with magnetite resulted in efficient CT contrast, which was superior to the conventional iodine-contrast agents. Cytotoxicity and oxidative stress analysis revealed the biocompatibility of this material even at high doses and long incubation periods. We anticipate that our results may gain fundamental importance in the development of nanohybrids for combinatorial medical applications, owing to the experimental demonstration of environmentally benign, nonpolluting synthesis procedure amenable to scale-ups.

ASSOCIATED CONTENT

Supporting Information

Contains additional FTIR, XPS, and particle stability analysis data. This material is available free of charge via the Internet at http://pubs.acs.org.

AUTHOR INFORMATION

Corresponding Author

*E-mail: deepthymenon@aims.amrita.edu or deepsmenon@gmail.com.

ACKNOWLEDGMENTS

This research work was financially support by the Nanomedicine grant from Indian Council of Medical Research (ICMR), Government of India, and the Nanotheragnostics

grant of the Department of Science and Technology, Government of India. We acknowledge the Nanotechnology Characterization Laboratory, Frederick, MD, for the TEM analysis and the Sophisticated Analytical Instrument Facility at IIT Chennai for the VSM measurements. We are grateful to Amrita Vishwavidyapeetham (Deemed University) for providing all infrastructural support for the research work.

REFERENCES

(1) Kickelbick, G. In *Hybrid Materials: Synthesis, Characterisation and Applications*, 1st ed.; Kickelbick, G., Ed.; Wiley-VCH: Weinheim, Germany, 2007; chapter 1, pp 1−48.
(2) Corot, C.; Robert, P.; Idée, J.-M.; Port, M. *Adv. Drug Delivery Rev.* **2006**, *58*, 1471.
(3) Roca, A. G.; Costo, R.; Rebolledo, A. F.; Veintemillas-Verdaguer, S.; Tartaj, P.; Gonźalez-Carreño, T.; Morales, M. P.; Serna, C. J. *J. Phys. D: Appl. Phys.* **2009**, *42*, 224002.
(4) Evans, C. W.; Raston, C. L.; Iyer, K. S. *Green Chem.* **2010**, *12*, 1175−1179.
(5) Lee, J. E.; Lee, N.; Kim, H.; Kim, J.; Choi, S. H.; Kim, J. H.; Kim, T.; Song, I. C.; Park, S. P.; Moon, W. K.; Hyeon, T. *J. Am. Chem. Soc.* **2010**, *132*, 552−557.
(6) Jin, Y.; Jia, C.; Huang, S.-W.; O ' Donnell, M.; Gao, X. *Nat. Commun. 1*, 41, DOI: 10.1038/ncomms1042.
(7) Smith, A. M.; Wen, M. M.; Nie, S. *Biochemistry* **2010**, *32*, 12.
(8) Hauck, T. S.; Anderson, R. E.; Fischer, H. C.; Newbigging, S.; Chan, W. C. W. *Small* **2010**, *6*, 138−144.
(9) Cai, Q.-Y.; Kim, S. H.; Choi, K. S.; Kim, S. Y.; Byun, S. J.; Kim, K. W.; Park, S. H.; Juhng, S. K.; Yoon, K.-H. *Invest. Radiol.* **2007**, *42*, 797−806.
(10) Shevchenko, E. V.; Bodnarchuk, M. I.; Kovalenko, M. V.; Talapin, D. V.; Smith, R. K.; Aloni, S.; Heiss, W.; Alivisatos, A. P. *Adv. Mater.* **2008**, *20*, 4323−4329.
(11) Yu, H.; Chen, M.; Rice, P. M.; Wang, S. X.; White, R. L.; Sun, S. *Nano Lett.* **2005**, *5*, 379−382.
(12) Wang, H.; Brandl, D. W.; Le, F.; Nordlander, P.; Halas, N. J. *Nano Lett.* **2006**, *6*, 827−832.
(13) Wei, Y.; Klajn, R.; Pinchuk, A. O.; Grzybowski, B. A. *Small* **2008**, *4*, 1635−1639.
(14) Kim, D.; Yu, M. K.; Lee, T. S.; Park, J. J.; Jeong, Y. Y.; Jon, S. *Nanotechnology* **2011**, *22*, 155101.
(15) Raveendran, P.; Fu, J.; Wallen, S. L. *J. Am. Chem. Soc.* **2003**, *125*, 13940−13941.
(16) Nune, S. K.; Chanda, N.; Shukla, R.; Katti, K.; Kulkarni, R. R.; Thilakavathy, S.; Mekapothula, S.; Kannan, R.; Katti, K. V. *J. Mater. Chem.* **2009**, *19*, 2912−2920.
(17) Yang, X.; Li, Q.; Wang, H.; Huang, J.; Lin, L.; Wang, W.; Sun, D.; Su, Y.; Opiyo, J.; Hong, L.; Wang, Y.; He, N.; Jia, L. *J. Nanopart. Res.* **2009**, *12*, 1589−1598.
(18) Nadagouda, M. N.; Varma, R. S. *Green Chem.* **2008**, *10*, 859−862.
(19) Moulton, M. C.; Braydich-Stolle, L. K.; Nadagouda, M. N.; Kunzelman, S.; Hussain, S. M.; Varma, R. S. *Nanoscale* **2010**, *2*, 763−770.
(20) Xiong, J.; Wang, Y.; Xue, Q.; Wu, X. *Green Chem.* **2011**, DOI: 10.1039/C0GC00772B.
(21) Bors, W.; Heller, W.; Michel, C.; Saran, M. *Methods Enzymol.* **1990**, *186*, 343−355.
(22) Lu, C-W; Hung, Y.; Hsiao, J-K; Yao, M.; Chung, T-H; Lin, Y-S; Wu, S-H; Hsu, S-C; Liu, H-M; Mou, C-Y; Yang, C-S; Huang, D-M; Chen, Y.-C. *Nano Lett.* **2007**, *7*, 149−154.
(23) Hsiao, J-K; Tai, M-F; Chu, H-H; Chen, S-T; Li, H; Lai, D-M; Hsieh, S-T; Wang, J-L; Liu, H-M *Magn. Reson. Med.* **2007**, *58*, 717−724.
(24) Wang, L.; Neoh, K-G; Kang, E-T; Shuter, B.; Wang, S.-C. *Biomaterials* **2010**, *31*, 3502−3511.
(25) Friedman, M.; Williams, L. D. *Bioorg. Chem.* **1974**, *3*, 267−280.
(26) Binulal, N. S.; Menon, D.; Selvamurugan, N.; Shalumon, K. T.; Suja, S.; Mony, U.; Jayakumar, R.; Nair, S. V. *Tissue Eng., Part A* **2010**, *16*, 393−404.
(27) Wilson, C. E.; Dhert, W. J.; van Blitterswijk, C. A.; Verbout, A. J.; de Bruijn, J. D. *J. Mater. Sci.−Mater. Med.* **2002**, *13*, 1265.
(28) Voytik-Harbin, S. L.; Brightman, A. O.; Waisner, B.; Lamar, C. H.; Badylak, S. F. *In Vitro Cell Dev. Biol. Anim.* **1998**, *34*, 239.
(29) Liu, Y-F; Yu, J.-S. *J. Colloid Interface Sci.* **2010**, *351*, 1−9.
(30) Polavarapu, L.; Manna, M.; Xu, Q.-H. *Nanoscale* **2011**, *3*, 429−434.
(31) Xu, Z.; Hou, Y.; Sun, S. *J. Am. Chem. Soc.* **2007**, *129*, 8698−8699.
(32) Daniel, M-C; Astruc, D. *Chem. Rev.* **2004**, *104*, 293.
(33) Xu, C.; Ho, D.; Xie, J.; Wang, C.; Kohler, N.; Walsh, E. G.; Morgan, J. R.; Chin, Y. E.; Sun, S. *Angew. Chem., Int. Ed.* **2008**, *47*, 173−176.
(34) Averitt, R. D.; Sarkar, D.; Halas, N. J. *Phys. Rev. Lett.* **1997**, *78*, 4217−4220.
(35) Hsieh, S.; Huang, B. Y.; Hsieh, S. L.; Wu, C. C.; Wu, C. H.; Lin, P. Y.; Huang, Y. S.; Chang, C. W. *Nanotechnology* **2010**, *21*, 445601.
(36) Henning, T. D.; Wendland, M. F.; Golovko, D.; Sutton, E. J.; Sennino, B.; Malek, F.; Bauer, J. S.; McDonald, D. M. *Magn. Reson. Med.* **2009**, *62*, 325−332.
(37) Popovtzer, R.; Agrawal, A.; Kotov, N. A.; Popovtzer, A.; Balter, J.; Carey, T. E.; Kopelman, R. *Nano Lett.* **2008**, *8*, 4593−4596.
(38) Ajeesh, M.; Francis, B. F.; John, A.; Varma, P. R. H. *J. Mater. Sci.-Mater. Med.* **2010**, *21*, 1427−1434.
(39) Gupta, A. K.; Gupta, M. *Biomaterials* **2005**, *26*, 3995−4021.
(40) Arbab, A. S.; Yocum, G. T.; Kalish, H.; Jordan, E. K.; Anderson, S. A.; Khakoo, A. Y.; Read, E. J.; Frank, J. A. *Blood* **2004**, *104*, 1217−1223.
(41) van Engeland, M.; Nieland, L. J.; Ramaekers, F. C.; Schutte, B.; Reutelingsperger, C. P. *Cytometry* **1998**, *31*, 1−9.
(42) Koga, T.; Moro, K.; Nakamori, K.; Yamakoshi, J.; Ho soyama, H.; Kataoka, S.; Ariga, T. *J. Agric. Food. Chem.* **1999**, *47*, 1892−1897.
(43) Bagchi, D.; Bagchi, M.; Stohs, S. J.; Ray, S. D.; Sen, C. K.; Preuss, H. G. *Ann. N.Y. Acad. Sci.* **2001**, *957*, 260−270.
(44) Houde, V.; Grenier, D.; Chandad, F. *J. Periodontol.* **2006**, *77*, 1371−1379.
(45) Han, Y.-S.; Bastianetto, S.; Dumont, Y.; Quirion, R. *J. Pharmacol. Exp. Ther.* **2006**, *318*, 238−245.